Active Thermal Protection System Against Intense Irradiation

S. Maruyama* and R. Viskanta†
Purdue University, West Lafayette, Indiana
and
T. Aihara‡
Tohoku University, Sendai, Japan

An active thermal insulation system for protecting a structure from intense incident radiation flux is considered. The system consists of a high-porosity semitransparent material through which a gas is transpired. A theoretical investigation is performed to study transient heat transfer by combined conduction, convection, and radiation in a layer of a semitransparent porous medium which is subjected to a high-intensity irradiation and injection of gas through the layer. Parametric calculations were performed and are reported in the paper. In the presence of gas injection through the porous layer, the temperature profile is totally different from that in the absence of injection, and the total heat flux through the layer vanishes within a small thickness. Drastic reduction in time to reach steady-state conditions is also achieved by the gas injection. The thickness of the porous layer and the radiation properties such as the single scattering albedo greatly affect the temperature distribution and the insulation performance.

Nomenclature

b, f = backward and forward scattering fractions
c_{pg}, c_s = specific heat of gas and porous material, J/kg K
d_p = equivalent particle diameter of porous media, m
E_1, E_2 = radiation fluxes leaving front and back surfaces of surroundings, σT_1^4, σT_2^4, Fig. 1, W/m^2
h_e = effective heat-transfer coefficient of porous media, W/m^{2}K
h_s = heat transfer coefficient at the front surface, W/m^{2}K
ℓ = thickness of porous layer, Fig. 1, m
k_a = apparent conductance of porous slab, $q_t\ell/(T_1-T_2)$, W/mK
k_m, k_g = thermal conductivity of porous media and gas, W/mK
n_a = apparent index of refraction, Eq. (16)
Nu_p = Nusselt number based on particle diameter, $h_e d_p/k_g$
N_R, N_c, N_g = radiation, heat advection, and convection parameters, Eqs. (4), (5), and (6), respectively
Pr = Prandtl number of gas, $\rho_g \nu c_{pg}/k_g$
q^+, q^- = forward and backward radiation fluxes, W/m^2
q_R = radiation flux, $q^+ - q^-$, W/m^2
q_s = convective heat flux at front surface, Fig. 1, W/m^2
q_t = total heat flux through porous media, Eq. (1), W/m^2
Q, Q^+, Q^- = dimensionless heat flux, $Q = q/(E_1-E_2)$, $Q^+ = q^+/(E_1-E_2)$, $Q^- = q^-/(E_1-E_2)$
Re_p = particle Reynolds number, $u_f d_p/\nu$
T_1, T_2 = radiation source temperatures at the front and back surfaces, Fig. 1, K
T_s, T_g = temperatures of porous media and gas, K
t = time, s
t^* = dimensionless time, $k_m t/(1-\phi)\rho_s c_s \ell^2$
u_f = superficial velocity of gas at entrance temperature, m/s
X = dimensionless length, x/ℓ
x_p = thermal penetration depth at steady-state condition, m
α = dimensionless heat-transfer coefficient, $|q_s|\ell/(T_1-T_2)k_m$
β = source temperature parameter, $(T_1/T_2)^4$
ϵ_s = surface emissivity of solid cross section at boundary, Fig. 1
θ_s, θ_g = dimensionless temperatures of porous media and gas, $(T_s-T_2)/(T_1-T_2)$, $(T_g-T_2)/(T_1-T_2)$
ν = kinematic viscosity of gas, m^2/s
ρ_s, ρ_g = true density of porous material and density of gas, kg/m^3
σ = Stefan–Boltzmann constant, W/m^{2}K^4
σ_e = extinction coefficient, 1/m
τ = optical depth, $\sigma_e x$
τ_o = optical thickness, $\sigma_e \ell$, Fig. 1
ϕ = porosity of porous media
ω_o = single scattering albedo of porous media

I. Introduction

THERMAL protection and insulation are important for the cooling of rocket nozzles and re-entry vehicles, protection of structures from high-intensity energy beams, and design of fusion reactors and furnaces for material processing. Broad surveys of the cooling and protection techniques are available.[1,2] When the boundaries of the system are exposed to a high-intensity irradiation and to a high-temperature environment, conventional insulating materials such as porous or fibrous media[3,4] have poor performance. This is especially true for steady-state conditions, because radiation heat transfer predominates over conduction.

Received Oct. 25, 1988; presented as Paper 89-0605 at the AIAA 27th Aerospace Sciences Meeting, Reno, NV, Jan. 8–10, 1989; revision received Feb. 13, 1989.

*Visiting Scholar, Heat Transfer Laboratory, School of Mechanical Engineering. Member AIAA.
†W. F. M. Goss Distinguished Professor of Engineering, Heat Transfer Laboratory, School of Mechanical Engineering. Associate Fellow AIAA.
‡Professor, Institute of High Speed Mechanics.

Considerable benefit is realized in mass-transfer cooling (transpiration, film, ablation) of thermal protection systems from the heat blockage due to the injection of material into the boundary layer.[5,6] For example, as the ablating material sublimes the ablation products pass through the permeable matrix and cause the desired heat-flux reduction. The advantages and disadvantages as well as practical problems with the different cooling methods and protection systems are well known[5-7] and need not be repeated here. Suffice it to mention that the heating loads (i.e., heat flux and duration of pulse) for planetary entry[1,2,7] and Earth-based[8] systems are different and so are the thermal protection system requirements. For example, it has been well documented that for short re-entry times the ablative systems are more efficient, whereas the transpiration and radiation schemes become more efficient as the entry times increase. In brief, the thermal protection system design depends on whether the convective, radiative or both heat loads are important and whether the duration of the load is short or long. The subject of this paper is to evaluate a scheme for protecting a structure from intense thermal irradiation over a long time period.

A high-performance thermal protection system capable of alleviating thermal damage can be achieved by using a semitransparent, highly scattering porous medium composed of a very fine structure through which a gas is transpired. The radiation absorbed by the medium is transferred to the gas by convection, which then transports a part of the heat away from the porous medium by advection.

There have been many studies of combined conduction-radiation heat transfer in porous media.[9] Heat transfer in a porous solid irradiated by an intense solar radiation flux was studied by Matthews et al.,[10] and a thermal conductance model was developed by Zumbrunnen et al.[11] A unique high-temperature heat-transfer augmentation scheme using porous media was proposed by Echigo,[12] and the application of this concept to combustion was studied by Echigo et al.[13]

Most of the studies concerned with transpiration cooling were intended to reduce the convective heat transfer between the ambient gas flow and the surface,[5] and few studies such as those of Epifanov and Leontjev[14] and Schuster[15] have treated heat transfer inside the porous material with transpiration in the absence of radiation. However, the authors could not identify any studies concerned with combined conduction-convection-radiation heat transfer in porous media with gas transpiration designed to thermally protect a structure.

In this paper, a theoretical investigation is performed to study transient heat transfer by combined conduction, convection, and radiation in a layer of a semitransparent, scattering porous medium which is subjected to high-intensity irradiation at one face and through which a gas is transpired. Parametric calculations were performed, and salient features of the thermal protection system are discussed.

II. Combined Heat-Transfer Model

A one-dimensional layer of a semitransparent high-porosity material as shown in Fig. 1 is considered. At the front surface of the plane, porous layer is exposed to high-intensity thermal radiation, and a low-temperature gas is injected through the back face of the layer. The radiation source at the front surface is characterized by temperature T_1, and the inlet gas temperature and ambient temperature at the back face is T_2. The front surface is subjected to a convective heat flux q_s, either from the exhaust or ambient gas.

For simplicity of the analysis, the porous material is assumed to be gray, and the thermophysical properties of the material and the gas are considered to be independent of temperature. The total heat flux q_t through the porous plane layer is given by

$$q_t = -k_m \frac{\partial T_s}{\partial x} + q_R - c_{pg}\rho_g u_f (T_g - T_2) \tag{1}$$

The first and second terms on the right-hand side of Eq. (1)

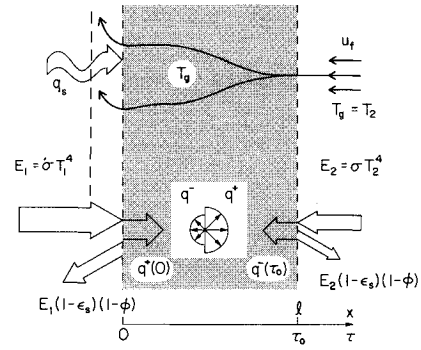

Fig. 1 Schematic of the physical model.

represent the conductive and radiative heat transfer, respectively, and the third term accounts for advective transport of energy by the transpired gas which flows through the porous medium. Since the heat capacity of the gas per unit volume is of the order 1/100–1/1000th of the porous medium, the transient term in the energy equation of the gas can justifiably be neglected. Also, the gas is considered to be radiatively nonparticipating. The mass flux $\rho_g u_f$ appearing in Eq. (1) is constant through the layer even though the gas is subjected to a large difference in temperature.

It is assumed that the porous medium can be represented by a packed bed of spherical monodisperse particles of diameter d_p. With this assumption, the surface area of the porous medium per unit volume becomes $6(1-\phi)/d_p$, and the heat is transferred from the particles to the transpired gas by convection. Introducing dimensionless parameters defined in the Nomenclature, the governing energy equations for the porous solid and the gas can be expressed as

$$\frac{\partial \theta_s}{\partial t^*} = \frac{\partial^2 \theta_s}{\partial X^2} - N_R \frac{\partial Q_R}{\partial X} + N_c \frac{\partial \theta_g}{\partial X} \tag{2}$$

$$\frac{\partial \theta_g}{\partial X} = -N_g(\theta_s - \theta_g) \tag{3}$$

where

$$N_R = \frac{\sigma(T_1^4 - T_2^4)}{k_m(T_1 - T_2)/\ell} = \frac{\sigma(T_1 + T_2)(T_1^2 + T_2^2)}{(k_m/\ell)} \tag{4}$$

$$N_c = \frac{c_{pg}\rho_g u_f \ell}{k_m} = \left(\frac{k_g}{k_m}\frac{\ell}{d_p}\right) PrRe_p \tag{5}$$

$$N_g = 6(1-\phi)\left(\frac{\ell}{d_p}\right)\frac{Nu_p}{PrRe_p} \tag{6}$$

As shown in Fig. 1, the surroundings of the layer are at ambient temperatures T_1 and T_2, and the front and back surfaces of the porous layer are subjected to the isotropic irradiation from blackbody sources at temperature T_1 and T_2, respectively. If the porosity of the medium is uniform and if the fraction of the cross-sectional area of the solid material on the surface of the porous slab is $(1-\phi)$, a fraction of the irradiation is absorbed by the solid cross section of the layer, and the remaining fraction penetrates into the medium. The absorption and emission of radiation by the solid exposed to the irradiation affect the boundary condition on the front and the back faces. Assuming that there is convective heat transfer at the front surface, the thermal boundary condition for the temperature of the porous medium is as follows:

$$-\frac{\partial \theta_s}{\partial X} = \frac{\ell(1-\phi)}{k_m(T_1 - T_2)}\epsilon_s \sigma\left[T_1^4 - T_s^4(0)\right] + \frac{\ell q_s}{k_m(T_1 - T_2)}, \qquad \text{at } X = 0 \tag{7}$$

The inlet gas temperature is assumed to be the same as that of the ambient temperature of the back face T_2, and the initial temperature of the porous medium is assumed to be T_2. Then,

$$-\frac{\partial\theta_s}{\partial X} = \frac{\ell(1-\phi)}{k_m(T_1-T_2)}\epsilon_s\sigma\left[T_s^4(1)-T_2^4\right], \qquad \text{at } X=1 \quad (8)$$

$$\theta_g = 0, \qquad \text{at } X=1 \quad (9)$$

$$\theta_g = \theta_s = 0, \qquad \text{for } t^*=0 \quad (10)$$

In the present analysis, with some extrapolation of the particle Reynolds number range, the empirical formula proposed by Huber and Jones[16] is adopted for the estimation of the effective heat-transfer coefficient:

$$Nu_p = 0.054Re_p^{1.48}, \qquad 0.7<Re_p<16 \quad (11)$$

The validity of the above equation and the comparison with the other empirical correlations are discussed in the literature.[17]

There have been many approximate methods proposed for predicting the radiant heat flux q_R. Menguc and Viskanta[18] have assessed the validity of several different methods by comparing the predictions with the exact solution, and the two-flux approximation was found to yield sufficiently accurate results for all optical thicknesses and scattering functions considered. As a consequence, the two-flux approximation is adopted in the analysis of the radiative transfer:

$$\frac{1}{2}\frac{dQ^+}{d\tau} = -(1-f\omega_o)Q^+ + \omega_o bQ^+ + (1-\omega_o)E_b \quad (12)$$

$$-\frac{1}{2}\frac{dQ^-}{d\tau} = -(1-f\omega_o)Q^- + \omega_o bQ^+ + (1-\omega_o)E_b \quad (13)$$

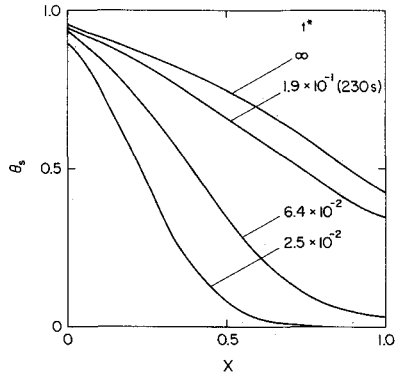

Fig. 2a Transient temperature distribution in porous media (radiation source temperature $T_1=2000$ K, inlet gas temperature $T_2=300$ K, thickness of the layer $\ell=10$ mm, $Re_p=5.0$, and $\alpha=0$).

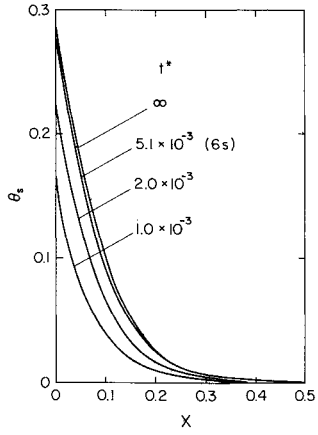

Fig. 2b Transient temperature distribution in porous media without gas injection ($T_1=2000$ K, $\ell=10$ mm, $Re_p=0$, and $\alpha=0$).

where

$$E_b = \frac{n_a^2\sigma T_s^4}{(E_1-E_2)} \quad (14)$$

Equation (2) and Eqs. (12) and (13) are related by

$$\frac{\partial Q_R}{\partial X} = 2\tau_o(1-\omega_o)(-Q^+-Q^-+2E_b) \quad (15)$$

The index of refraction n_a appearing in Eqs. (12) and (13) needs special treatment when the material, such as a porous medium, is inhomogeneous. In the present analysis, the effective index of refraction n_a as originally derived by Maxwell-Garnett is calculated from the following expression[19]:

$$n_a^2 = n_g^2\left[\frac{n_s^2+2n_g^2+2(1-\phi)(n_s^2-n_g^2)}{n_s^2+2n_g^2-(1-\phi)(n_s^2+n_g^2)}\right] \quad (16)$$

Recalling the gray assumption and the discussion of the boundary conditions in Eqs. (7) and (8), the boundary conditions for the radiative fluxes can be expressed as

$$Q^+ = \left[\phi+\epsilon_s(1-\phi)\right]\frac{E_1}{E_1-E_2}, \qquad \text{at } \tau=0 \quad (17)$$

$$Q^- = \left[\phi+\epsilon_s(1-\phi)\right]\frac{E_2}{E_1-E_2}, \qquad \text{at } \tau=\tau_o \quad (18)$$

where the internal reflection by the solid boundary for the radiation incident from inside the material is neglected.

The solution of Eqs. (2), (3), (12), and (13) was obtained numerically using a finite-difference scheme with an iterative procedure. Discussion of the present model and the numerical procedure is available elsewhere.[17]

III. Results and Discussion

Porous zirconia was chosen as the medium for the numerical calculations. The working fluid was selected to be air at 30 K and 1 atm. There are few sources of data available in the literature for porous materials for which both thermal and radiation properties were measured or estimated. A high-porosity, high-temperature porous material used by Matthews et al.[10] was chosen as a porous medium. The thermophysical and radiative properties of the porous medium are listed in Table 1. The porosity, $\phi=0.9$, and characteristic particle diameter, $d_p=100$ μm, were assumed.

Transient Temperature Distribution

The transient temperature distributions in the porous medium with gas transpiration are plotted in Fig. 2a. In this example, the temperature of the radiation source T_1 was chosen to be 2000 K so that the irradiation at the front surface would be approximately 1 MW/m^2. The Reynolds number, $Re_p=5.0$, corresponds to the superficial velocity of $u_f=0.79$ m/s. For the purpose of comparison, the temperature distribution in the solid in the absence of gas transpiration through the matrix ($Re_p=0$) is also plotted in Fig. 2b.

Comparison of Figs. 2a and 2b reveals that the injection of the gas through the porous layer not only gives totally different temperature profiles, but also greatly affects the time to reach steady-state conditions. If we define the time to reach steady state t_{ss}^* as

$$\left|\frac{\partial\theta_s}{\partial t^*}(t_{ss}^*, x=0,1)\right| < 10^{-3} \quad (19)$$

then the dimensionless times for $Re_p=5.0$ and 0 are 2.25×10^{-2} (27 s) and 6.2×10^{-1} (750 s), respectively. A drastic reduction in the time to reach steady state is found when a gas is transpired, i.e., the dimensionless time is approximately 30 times shorter than in the absence of gas transpiration.

Table 1 Thermophysical and radiation properties of porous zirconia

Thermophysical properties
$c_s = 1.75 \times 10^3$ J/kg · K
$\rho_s = 5.60 \times 10^3$ kg/m^3
$\rho = (1-\phi)\rho_s = 5.6 \times 10^2$ kg/m^3 (where $\phi = 0.9$ is assumed)
$k_m = 8.2 \times 10^{-2}$ W/mK ($T_s = 600$ K)
$d_p = 100\mu$m $= 10^{-4}$m (assumed)
Radiation properties
$\sigma_e = 8.969 \times 10^3$ m^{-1}
$b = 0.2506$
$\omega_o = 0.99$
$n_s = 1.6$, $n_g = 1.0$
$n_a = 1.05$, ($n_a^2 = 1.11$)
$\epsilon_s = 0.35$

In the present analysis, the steady-state thermal penetration depth x_p is defined as the thickness where the steady-state solid temperature is reduced to a value of $\theta_s = 0.01$. If x_p is less than the thickness of the porous layer ℓ, the effective thickness of the porous layer becomes x_p. If one recalls that the dimensionless time t^* is inversely proportional to ℓ^2 and compares the steady-state temperature distributions in Fig. 2, one can conclude that the smaller the effective depth of the thermal penetration in the porous layer, the shorter is the time to reach steady state. The results suggest that for an active thermal protection system both the insulation thickness and the heat-up time are decreased significantly. The decrease in heat-up time can shorten the turnaround time of large and even small (i.e., used in new materials processing) industrial furnaces.

Steady-State Temperature Distribution and Heat Flux

The effects of gas injection on the temperature distribution in the porous solid and gas are shown in Fig. 3. The boundary conditions are the same as those employed to obtain the results reported in Fig. 2. The injection of the gas greatly changes the temperature distribution in the porous medium, relative to the case without gas injection. Especially remarkable is the decrease of the back-surface temperature $\theta_s(1)$, even for the very low superficial gas velocity. Also, the temperature at the front surface can be greatly reduced for $Re_p = 5.0$.

It can be noted from the temperature distribution for $Re_p = 5.0$ that the thickness of the layer can be reduced to as small as 5 mm without increasing the total heat-transfer rate at the front surface. The large difference between the solid and gas temperatures at the front surface implies that the assumption $\theta_g = \theta_s$ adopted by some authors in the literature for heat transfer in porous media is not appropriate for the present problem when the porous material is exposed to a very intense incident radiation flux.

Under steady-state conditions, the local dimensionless heat flux [see Eq. (1)] is constant, i.e.,

$$Q_t = -\frac{1}{N_R}\frac{\partial \theta_s}{\partial X} + Q_R - \frac{N_c}{N_R}\theta_g \qquad (20)$$

For this limiting case, the steady-state conductive, advective, and radiative fluxes for $Re_p = 5.0$ and 0 are plotted in Figs. 4a and 4b, respectively. In the figure, Q_{cd} and Q_{cv} are the first and third terms of the right-hand side in Eq. (20). The boundary conditions given in the figures are the same as those in Fig. 3. It is noted that the total heat flux through the porous layer almost vanishes for $Re_p = 5.0$. The conductive heat flux is a much smaller fraction of the total heat flux than the radiative or convective fluxes, because the radiation transfer parameter N_R is 65. On the other hand, the advective heat flux Q_{cv} is of comparable magnitude to the radiative flux. The radiative fluxes Q^+ and Q^- are unsymmetric (Fig. 4a). Each flux almost vanishes at $X = 0.3$ ($x = 3$ mm). This trend is similar to the temperature distribution shown in Fig. 3a. However, in the absence of gas injection (Fig. 4b) the heat fluxes remain finite at the back face. It is noted that for conventional insulation (Fig. 4b), the heat transfer through the insulation does not vanish (even though it is very small) to maintain the outer surface at a desired temperature. However, the present active insulation system (Fig. 4a) can eliminate heat transfer through the system by maintaining the exposed front surface at a low temperature.

Effects of Surface Heat Flux

In transpiration cooling, the transpired gas is intended to reduce the convective heat transfer at the front surface.[5] Many existing studies are concerned with heat transfer between the surface and ambient gas flow in which the injected gas is assumed to be at the same temperature as the wall. This assumption is appropriate if the particle diameter is small and

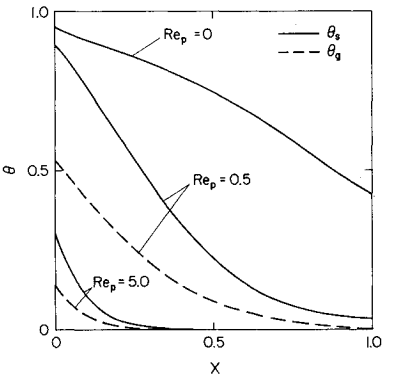

Fig. 3 Effects of gas injection on the dimensionless temperature distribution in the solid and gas ($T_1 = 2000$ K, $\ell = 10$ mm, and $\alpha = 0$).

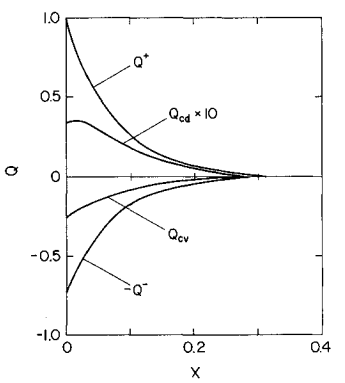

Fig. 4a Steady-state dimensionless radiative fluxes Q^+, Q^-, conductive flux Q_{cd}, and advective flux Q_{cv} ($Re_p = 5.0$, $T_1 = 2000$ K, $\ell = 10$ mm, and $\alpha = 0$).

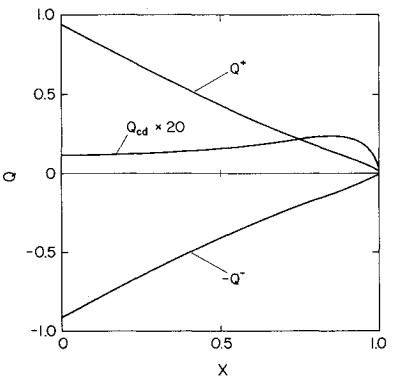

Fig. 4b Steady-state dimensionless radiative fluxes Q^+, Q^-, and conductive flux Q_{cd} without gas injection ($Re_p = 0$, $T_1 = 2000$ K, $\ell = 10$ mm, and $\alpha = 0$).

irradiation is absent.[15] However, for a porous layer subjected to very high intensity irradiation on the front surface, the thermal equilibrium assumption is not appropriate as shown in Fig. 3, and low temperature gas [$\theta_g(0) < \theta_s(0)$] leaves the front surface of the layer. For this case, the heat flux might be positive (from ambient to the surface) or negative (from surface to ambient). There are no experimental data or analysis for such a case, either for natural convection or for forced convection.

The effect of dimensionless surface heat flux $Q_s[=q_s\ell/(T_1-T_2)k_m]$ on the solid temperature distribution is shown in Fig. 5. Here, the dimensionless heat-transfer coefficient α is chosen to be 10, which corresponds to a convective heat-transfer coefficient of 82 W/m^{2}K. In the figure, the value for the case of $\alpha=0$ is also presented. The effect of the surface heat flux is to raise or lower the temperature near the front surface; however, this effect is restricted to within 10% of the layer thickness, and the remaining region is not affected by the convective heat transfer at the front face. This fact implies that the apparent thermal conductivity or the total heat flux is not affected by the surface heat flux.

Effects of Other Parameters

The solid temperature at the front and back surfaces [$\theta_s(0)$ and $\theta_s(1)$], the exit gas temperature $\theta_g(0)$, and aparent steady-state conductance k_a are plotted for different parameters in Figs. 6–9. The dimensionless apparent conductance is related to the dimensionless total heat flux Q_t by

$$k_a/k_m = N_R Q_t \tag{21}$$

Figure 6 shows the effects of gas-injection velocity on the temperatures in the gas and solid and on the apparent conductance. The solid temperatures at the two faces of the layer [$\theta_g(0)$ and $\theta_s(1)$], along with k_a/k_m, increase with a decrease in the gas velocity. The exit gas temperature $\theta_g(0)$, on the other hand, has a maximum around $Re_p=0.7$ ($u_f=0.11$ m/s). This maximum is due to the convection heat-transfer coefficient model between the solid particles of the porous bed and the gas [i.e., Eq. (11)]. In the absence of gas injection ($Re_p=0$), the apparent conductance is 1.6 times higher than the thermal conductivity of the solid matrix. Once the injection starts, the conductance decreases to about one-seventh of the thermal conductivity of the solid for $Re_p>2$. Further increases in the gas-injection velocity do not affect the conductance. This trend is similar to that of the temperature of the solid at the back surface.

Figure 7 shows the effects of the porous-layer thickness. If the layer is more than 5 mm thick, the exit-gas and the front-surface temperatures are constant, and the heat transfer through the material is completely eliminated. This thickness corresponds to the thermal penetration depth discussed in Figs. 3 and 4. Abrupt changes in surface and gas temperatures are observed for a layer less than 3 mm thick. The increase in the apparent conductance is also significant. This is due to the fact that the material is not thick enough to attenuate the incident radiation flux and that the surface area is too small to transfer the absorbed energy by convection to the gas. In order to utilize the proposed active insulation system, a certain thickness of the porous layer is needed, although it may be very small compared with that of the conventional insulation.

The effects of the intensity of incident radiation flux q_1 are shown in Fig. 8. In the figure, two different parameters, $\beta=(T_1/T_2)^4$, where $T_2=300$ K, and $E_1=\sigma T_1^4$, are used as the abscissas. The particle Reynolds number and layer thickness are chosen as 3 ($u_f=0.47$ m/s) and 3 mm, respectively. A sudden increase in k_a/k_m is evident for high heat fluxes, especially for $\beta>10^4$. Also, the front-surface temperature is quite high in this range. This is due to the fact that the thermal penetration

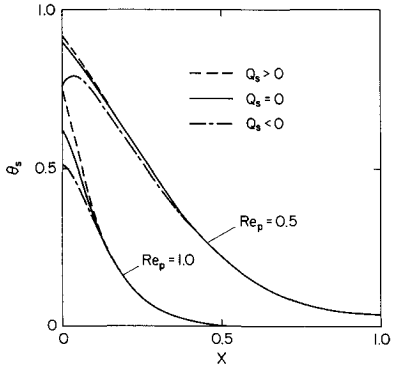

Fig. 5 Effects of convective heat transfer at the front surface on the steady-state temperature distribution in the solid for $\alpha=10$.

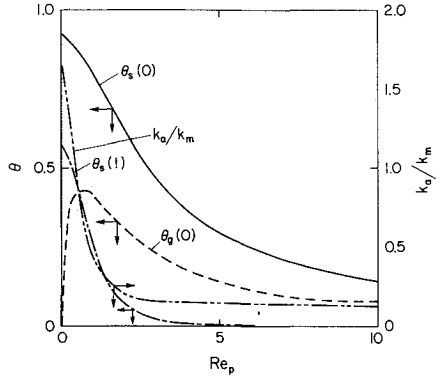

Fig. 6 Effects of gas-injection velocity on solid temperature at the front [$\theta_s(0)$] and back [$\theta_s(1)$] surfaces, exit-gas temperature $\theta_g(0)$, and dimensionless apparent conductance k_a/k_m ($T_1=2000$ K, $\ell=3$ mm, and $\alpha=0$).

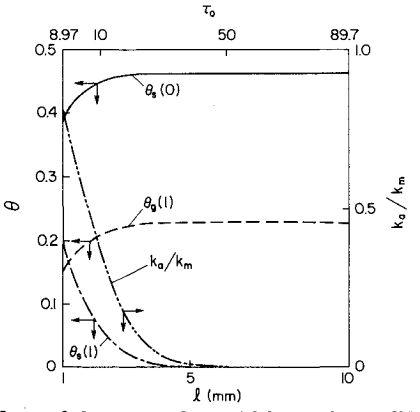

Fig. 7 Effects of the porous-layer thickness ℓ on solid temperatures at the front and back surfaces, exit-gas temprature, and dimensionless apparent conductance ($Re_p=3.0$, $T_1=2000$ K, and $\alpha=0$).

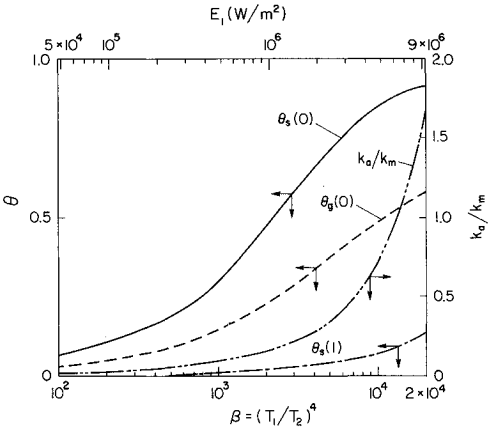

Fig. 8 Effects of radiation source temperature T_1 on the solid temperatures at the front and back surfaces, exit-gas temperature, and dimensionless apparent conductance ($Re_p=3.0$, $\ell=3$ mm, and $\alpha=0$).

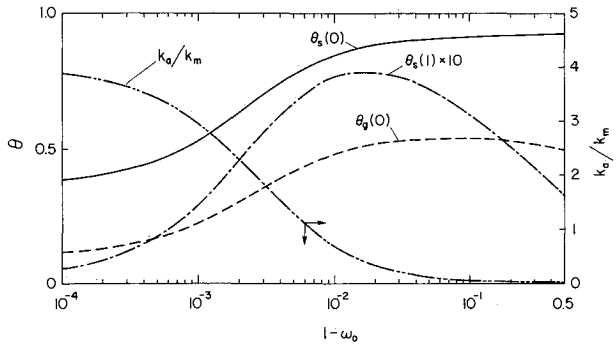

Fig. 9 Effects of single-scattering albedo ω_o on the solid temperature at the front and back surfaces, exit-gas temperature, and dimensionless apparent conductance ($Re_p = 3.0$, $T_1 = 3000$ K, $T_1/T_2 = 10$, $\ell = 3$ mm, and $\alpha = 0$).

depth is too large, and the layer is too thin to attenuate the incident radiation flux. A material having a larger scattering albedo is more effective for reducing the front-surface temperature, as will be shown in Fig. 9. For such a high-temperature condition, use of a dissociating gas might be effective to increase the heat capacity of the gas.

The preceding results are for a porous material having a single scattering albedo of $\omega_o = 0.99$. The albedo is considered to be a model parameter while the remaining parameters are the same as those given in Table 1. The calculated surface temperatuers and apparent conductance are shown in Fig. 9. When $(1-\omega_o)$ is small, the radiation absorbed by the material is small, and so is the exit-gas temperature. The predicted conductances are rather large; however, the surface temperature of the material remains low for small $(1-\omega_o)$. The opposite can be said for large $(1-\omega_o)$. These trends are closely related to the radiant energy absorbed by the material and the thermal penetration depth. When $(1-\omega_o)$ is small, the penetration depth is large, but the energy absorbed by the material and transferred to the gas is small. On the other hand, the thermal penetration depth is small for large $(1-\omega_o)$, and there is not sufficient depth (area) to transfer the absorbed energy to the gas by convection. The results show that there is a maximum gas temperature at $(1-\omega_o) \approx 0.1$. It is noted that there is little difference in conductance and front-face temperature for albedos in the range $0.5 < \omega_o < 0.9$.

IV. Conclusions

A theoretical investigation of transient heat transfer by combined conduction, convection, and radiation in a layer of a semitransparent porous medium was performed. Gas injection through the layer not only changes the temperature distribution in the solid matrix, but also substantially shortens the time necessary to reach the steady-state condition. When the gas is injected, the time required to reach steady state is approximately 30 times shorter than that without gas injection.

Heat-transfer rate through the insulating boundary vanishes with the gas injection, while maintaining the boundary at a very low temperature. This condition can be achieved within a 5-mm-thick layer for an incident radiation flux of 1 MW/m^2 and gas velocity of 0.8 m/s. Under steady-state conditions, when the front surface is subjected to high-intensity irradiation, the conductive heat flux is small compared with the radiative and advective fluxes.

There can be a large temperature difference between the solid at the front surface and the exhausted gas. This fact suggests that the assumption of thermal equilibrium between the gas and the porous solid is inappropriate for the present problem where the porous material is exposed to a very intense thermal radiation flux.

Gas-injection velocity and layer thickness (even though it is very thin) substantially affect the front-surface temperature of the solid and the insulation performance. However, convective heat transfer at the front surface only affects the temperature distribution within 10% of the layer and does not affect the insulation performance. The single scattering albedo of the porous material strongly influences the performance of the insulation. The front-surface temperature is low for large albedos, whereas there is little difference in the characteristics for albedos between 0.9 and 0.5.

When the radiation source temperature and irradiation become large (i.e., larger than 5.0 MW/m^2), larger layer thicknesses and larger albedos are required in order to achieve good insulation and thermal protection.

References

[1]Sutton, G. P., Wagner, W. R., and Seader, J. D., "Advanced Cooling Techniques of Rocket Engines," *Aeronautics & Astronautics,* Vol. 4, Jan. 1966, pp. 60–71.

[2]Sones, P. D. and Rossi, J. J., "A Study of Advanced Thermal Protection Systems," AIAA Paper 68-300, April 1968.

[3]Tong, T. W., Yang, Q. S., and Tien, C. L., "Radiative Heat Transfer in Fibrous Insultations—Part II: Experimental Study," *ASME Journal of Heat Transfer,* Vol. 105, No. 1, Feb. 1983, pp. 76–81.

[4]Rish, J. W., III, and Roux, J. A., "The Effect of Radiation Barriers on Conduction and Radiation Heat Transfer in Fibrous Insulations," *Proceedings of the 8th International Heat Transfer Conference,* Hemisphere, Washington, D.C., Vol. 2, 1986, pp. 721–726.

[5]Hartnett, J. P., "Mass-Transfer Cooling," *Handbook of Heat-Transfer Applications,* 2nd ed., edited by W. M. Rosenow, J. P. Hartnett, and E. N. Ganic, McGraw-Hill, New York, 1985, pp. 1-1–1-109.

[6]Hurwicz, H. and Rogan, J. E., "Ablation," *Handbook of Heat Transfer,* edited by W. H. Rosenow and J. P. Hartnett, McGraw-Hill, New York, 1973, Section 16.

[7]Polezhaev, Yu. V. and Yurevich, F. B., *Thermal Protection,* "Energiya," Moskva, 1976 (in Russian).

[8]Yano, T., Matsushima, E., and Fuchigami, S., "Thermal Protection for Disaster Prevention Robot by Transpiration Cooling," *Proceedings of the 25th National Heat Transfer Symposium of Japan,* Vol. 2, 1988, pp. 187–189 (in Japanese).

[9]Chan, C. K. and Tien, C. L., "Combined Radiation and Conduction in Packed Spheres," *Proceedings of the 5th Internatioanl Heat Transfer Conference,* Vol. 1, American Society of Mechanical Engineers, 1974, pp. 72–74.

[10]Matthews, L. K., Viskanta, R., and Incropera, F. P., "Combined Conduction and Radiation Heat Transfer in Porous Materials Heated by Intense Solar Radiation," *ASME Journal of Solar Energy Engineering,* Vol. 107, Feb. 1985, pp. 29–34.

[11]Zumbrunnen, D. A., Viskanta, R., and Incropera, F. P., "Heat Transfer Through Porous Solids with Complex Internal Geometries," *International Journal of Heat and Mass Transfer,* Vol. 29, Feb. 1986, pp. 275–282.

[12]Echigo, R., "High Temperature Heat Transfer Augmentation," *High Temperature Heat Exchangers,* edited by Y. Mori, A. E. Sheindlin, and N. Afgan, Hemisphere, Washington, D.C., 1986, pp. 230–259.

[13]Echigo, R., Yoshizawa, Y., Hanamura, K., and Tomimura, T., "Analytical and Experimental Studies on Radiative Propagation in Porous Media with Internal Heat Generation," *Proceedings of the 8th International Heat Transfer Conference,* Vol. 2, Hemisphere, Washington, D.C., 1986, pp. 827–832.

[14]Epifanov, V. M. and Leontjev, A. I., "Heat and Mass Transfer in Transpiration Cooled Turbine Blades," *Proceedings of the 7th International Heat Transfer Conference,* Vol. 6, Hemisphere, Washington, D.C., 1982, pp. 61–65.

[15]Schuster, J. R., "Nonisothermal Porous Flow in Transpiration-Cooled Nosetips," *Proceedings of the 5th International Heat Transfer Conference,* Vol. 5, Hemisphere, Washington, D.C., 1974, pp. 93–97.

[16]Huber, M. L. and Jones, M. C., "A Frequency-Response Study of Packed-Bed Heat Transfer at Elevated Temperatures," *International Journal of Heat and Mass Transfer,* Vol. 31, April 1988, pp. 843–853.

[17]Maruyama, S., Viskanta, R., and Aihara, T., "An Active Thermal Insulation System Using Semitransparent Porous Media for Protection Against Intense Irradiation," AIAA Paper 89-0605, Jan. 1989.

[18]Menguc, M. P. and Viskanta, R., "Comparison of Radiative Transfer Approximations for a Highly Forward Scattering Planar Medium," *Journal of Quantitative Spectroscopy and Radiative Transfer,* Vol. 29, May 1983, pp. 381–394.

[19]Reiss, H., *Radiative Transfer in Nontransparent, Dispersed Media,* Springer-Verlag, Berlin, 1988, pp. 136–138.